# The electronic structure of ZrCl

R. S. Ram
*Department of Chemistry, University of Arizona, Tucson, Arizona 85721*

A. G. Adam and W. Sha
*Department of Chemistry, University of New Brunswick, Fredericton, NB E3B 6E2, Canada*

A. Tsouli and J. Liévin
*Université Libre de Bruxelles, Laboratoire de Chimie Physique Moléculaire, CP 160/09, Av. F.D. Roosevelt 50, Bruxelles, Belgium*

P. F. Bernath
*Department of Chemistry, University of Arizona, Tucson, Arizona 85721 and Department of Chemistry, University of Waterloo, Waterloo, ON N2L 3G1, Canada*

(Received 28 August 2000; accepted 6 December 2000)

The proposed electronic assignments of our previously reported near infrared transitions of ZrCl [J. Mol. Spectrosc. **186**, 335 (1997); **196**, 235 (1999)] have been revised following the suggestion of Sakai, Mogi, and Miyoshi [J. Chem. Phys. **111**, 3989 (1999)]. The ground state is now assigned as the $X\,^2\Delta$ state followed by the $a\,^4\Phi$ state being the lowest in the quartet manifold. The previously reported transitions $[7.3]^2\Delta-a\,^2\Phi$, $[9.4]^2\Phi-a\,^2\Phi$, and $C\,^4\Delta-X\,^4\Phi$ are now reassigned to $C\,^2\Phi-X\,^2\Delta$, $E\,^2\Phi-X\,^2\Delta$, and $d\,^4\Delta-a\,^4\Phi$, respectively. The new assignments are supported by our own *ab initio* calculations. Laser excitation spectra of the 414 nm band system have also been observed at low resolution and are attributed to a $^4\Gamma-a\,^4\Phi$ transition. © *2001 American Institute of Physics.* [DOI: 10.1063/1.1343904]

## I. INTRODUCTION

The electronic spectra of TiCl, ZrCl, and HfCl have recently been analyzed. In general, there is good agreement between the experimental observations and *ab initio* calculations, with the exception of ZrCl. Sakai, Mogi, and Miyoshi[1] in their recent theoretical paper on TiCl and ZrCl suggested that our[2] electronic assignments for ZrCl should be reconsidered. We have decided to do so by carrying out our own *ab initio* calculations and by recording some new laser excitation spectra of ZrCl.

The first spectroscopic investigation on ZrCl was carried out by Carroll and Daly[3] in 1961. They found three band systems in the near UV region and called them $A(284-291\,\text{nm})$, $B(363-380\,\text{nm})$, and $C(404-415\,\text{nm})$. No rotational analysis could be carried out and system *C* was similar to the corresponding TiCl system near 410 nm.[4] System *C* was also recorded by Jordan *et al.*[5] using a corona-excited supersonic jet source, but again no rotational structure was resolved. These two groups[3,5] suggested that the 410 nm bands were due to a $^4\Pi-^4\Sigma^-$ transition, but this assignment is almost certainly not correct. Imajo *et al.*[4] have demonstrated that the corresponding transition in TiCl is $^4\Gamma-X\,^4\Phi$ and have recorded similar emission spectra for ZrCl.

The electronic structure of the isovalent TiCl and HfCl molecules provides some guidance for ZrCl. The ground state of TiCl is established as $X\,^4\Phi$ by both experiment[6,7] and theory.[1,8,9] Although the TiCl $C\,^4\Delta-X\,^4\Phi$, $G\,^4\Phi-C\,^4\Delta$, and $G\,^4\Phi-X\,^4\Phi$ near infrared electronic transitions were recorded in emission,[6] the *ab initio* predictions of a $X\,^4\Phi$ ground state are unambiguous.[1,8,9] In addition, pure rotational spectra[7] of all four spin components confirm the $X\,^4\Phi$ assignment. Very recently we have measured the $[17.1]^2\Delta_{3/2}-X\,^2\Delta_{3/2}$ and $[7.6]^4\Delta_{3/2}-X\,^2\Delta_{3/2}$ transitions of HfCl, and carried out *ab initio* calculations to guide our interpretation of the spectra.[10] The ground state of HfCl was demonstrated to be a regular $^2\Delta$ state both by calculation and by measuring the $[17.1]^2\Delta_{3/2}-X\,^2\Delta_{3/2}$ transition in absorption.[10] Zr lies between Ti and Hf in the Periodic Table and the low-lying $^4\Phi$ and $^2\Delta$ states of ZrCl are essentially isoenergetic.[1] A ZrCl $^4\Delta\rightarrow{}^4\Phi$ infrared electronic transition[2] was recorded near 4000 $\text{cm}^{-1}$. By comparison with the analogous transition in TiCl,[6] this transition was labeled as the $C\,^4\Delta-X\,^4\Phi$ transition and the lower state was assumed to be the ground state.[2] Experiments and calculations now show that this assumption was incorrect and the transition needs to be relabeled as $d\,^4\Delta-a\,^4\Phi$.

Two other infrared electronic transitions were also measured previously and assigned as doublet transitions.[11,12] Partly on the basis of some unpublished ligand field calculations,[13] these transitions were tentatively labeled as $[7.3]^2\Delta-a\,^2\Phi$ and $[9.4]^2\Phi-a\,^2\Phi$ transitions. Our new *ab initio* calculations now establish these transitions to be $C\,^2\Phi-X\,^2\Delta$ and $E\,^2\Delta-X\,^2\Delta$, respectively. Note that, as mentioned in the discussion of Ram and Bernath,[11] these new assignments are also consistent with the observations. This paper describes the *ab initio* calculations and experiments that led to the reinterpretation of our previous measurements.

## II. EXPERIMENTAL DETAILS

The intent behind recording new spectra for ZrCl was to determine the nature of the *C* band system seen by Carroll

 

and Daly[3] and Jordan *et al.*[5] because the electronic assignment of this transition ($^4\Pi - ^4\Sigma^-$) proposed by these authors is incorrect. The apparatus used to create the ZrCl molecules has been used in our previous studies of transition halide molecules[10,14] so only a brief description of the equipment, pertinent to this experiment, will be given here.

A slowly rotating and translating zirconium rod situated in front of a pulsed molecular beam valve was ablated with about 4–6 mJ of 355 nm radiation from a pulsed Nd:YAG laser. At the same time, a gas mixture of about 4% $CCl_4$ or $CHCl_3$ seeded in He was passed through the valve into the ablation region. Vaporized Zr atoms were entrained in the gas mixture and expanded through a short expansion channel into the vacuum chamber producing a molecular jet.

The ZrCl molecules were formed through reaction of the hot Zr atoms with the $CCl_4$ or $CHCl_3$ molecules and their decomposition products during the expansion process. About 5 cm downstream from the nozzle orifice, the molecular beam was probed with a pulsed tunable dye laser. Laser-induced fluorescence was collected orthogonally to both the molecular beam and probe laser beam directions. The light was imaged onto a 0.25 m monochromator and detected by a cooled photomultiplier tube. The signal was amplified, integrated and sent to a computer controlling the laser system. The dyes, Stilbene 420, and Exalites 417, 411, and 404, were used to search for the *C* band system. Calibration of the pulsed laser data was accomplished using the numerous Zr atomic lines seen in the spectra and the wavelengths from the MIT wavelength tables.[15] The measurement accuracy is estimated to be about $\pm 0.1$ cm$^{-1}$.

## III. *AB INITIO* CALCULATIONS

Large scale *ab initio* calculations have been performed in order to investigate the valence electronic structure of ZrCl. The potential energy curves and the spectroscopic properties of 19 low-lying electronic states have been calculated using the same computational approach as in our recent work on the isovalent HfCl molecule.[10] Molecular orbitals optimized by state-averaged full-valence CASSCF calculations[16] are used as input for internally-contracted multireference configuration interaction (CMRCI) calculations[17] correlating all valence electrons. Davidson's corrections[18] for four-particle unlinked clusters are added to the CMRCI energies. Both atoms are described by quasirelativistic Wood–Boring pseudopotentials with 28 and 10 core electrons for the Zr and Cl atoms, respectively.[19,20] The corresponding valence double zeta basis sets[19,20] are augmented by a single Gaussian polarization orbital on each atom (*f*-type function with an exponent of 0.8 on Zr and *d*-type function with an exponent of 0.75 on Cl). The valence orbital space is defined by the four $\sigma$, two $\pi$, and one $\delta$ molecular orbitals arising from the $4d$ and $5s$ orbitals of Zr and the $3s$ and $3p$ orbitals of Cl. The two $\sigma$ and the $\pi$ orbitals correlating to the $4s$ and $4p$ orbitals of Zr were kept closed in all calculations. The size of the CASSCF (CMRCI) wave functions ranges from 5000 to 7000 (660 000 to 780 000) configuration state functions ($C_{2v}$ symmetry) depending on the space and spin symmetries.

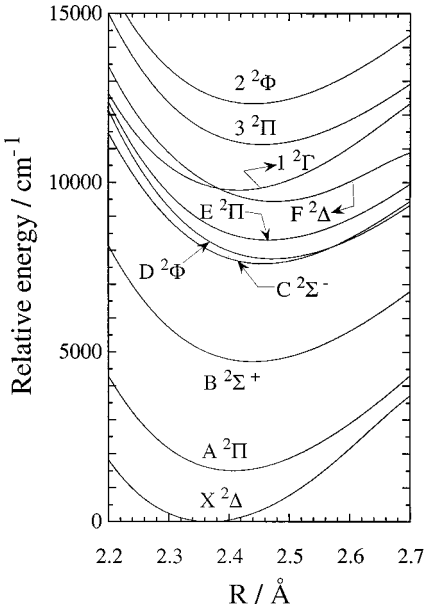


FIG. 1. The low-lying doublet potential energy curves of ZrCl from CMRCI calculations.

For comparison purposes, vertical term energies were also calculated for the isovalent HfCl and TiCl molecules (see Sec. V), using the same CASSCF/CMRCI computational procedure explained above (see also Ref. 10). The only difference is the use of a quasirelativistic pseudopotential (60 core electrons) for Hf (Ref. 19) and a relativistic Dirac–Fock pseudopotential (10 core electrons) for Ti.[21] The basis sets for both atoms are those of the corresponding core potentials from the Stuttgart library.[19,21] All calculations were performed with the MOLPRO package[22] running on the Compaq alpha servers of the ULB/VUB computer center.

## IV. ELECTRONIC STRUCTURE OF ZrCl FROM *AB INITIO* CALCULATIONS

The potential energy curves of 19 low-lying electronic states of ZrCl have been obtained from CMRCI calculations performed at 11 internuclear distances equally distributed between 2.2 and 2.7 Å. Figures 1 and 2 show the potential curves of 10 low-lying doublet and 9 low-lying quartet states, respectively. The energy scale of both figures is relative to the minimum energy of the ground electronic state, predicted here to be of $^2\Delta$ symmetry. The spectroscopic properties calculated from all these curves are given in Table I, where the following properties are reported: the equilibrium internuclear distances $R_e$, the harmonic frequencies at equilibrium $\omega_e$ and the term energies $T_0$, corrected for the zero point energy contribution calculated within the harmonic approximation. The discussion of the assignment of observed transitions and the comparison between calculated and experimental values will be given below (see Sec. VII). The relative energies between both spin systems are better illustrated in Fig. 3, where the $T_0$ energy values are used. The arrows correspond to previously observed transitions (see discussion in Sec. VII). Different clusters of levels, labeled from I to VI, are marked in this figure. Such clustering was also observed in the HfCl molecule[10] and it is also

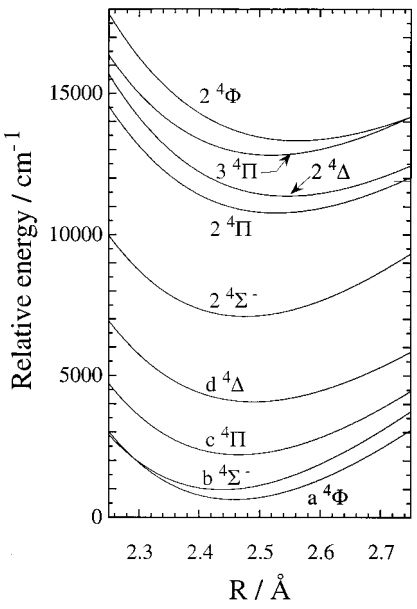


FIG. 2. The low-lying quartet potential energy curves of ZrCl from CMRCI calculations.

present in TiCl (see Sec. V). As shown before,[10] this clustering helps in the interpretation of the low-lying electronic structure of transition metal halides. Each cluster corresponds to a given class of configurations and to a given spin multiplicity. The relationship between clusters and configuration classes can easily be deduced by analysis of the CMRCI wave functions presented in Tables II and III.

Table II gives a list of 15 configurations, labeled from (A) to (O), which have a weight greater than or equal to 2% in the CMRCI wave functions, as detailed in Table III. The configuration weights are calculated as the squares of the corresponding CI coefficients. Table II characterizes each configuration in terms of electron promotions with respect to the ground configuration ($1\sigma^2 2\sigma^2 1\pi^4 3\sigma^2 1\delta^1$) and also reports the arising electronic states.

Let us start from the one electron picture provided by the CASSCF molecular orbital energies. As in HfCl,[10] one finds that $\{1\delta, 2\pi, 4\sigma\}$ form a set of quasi-isoenergetic orbitals (within 1 eV) separated from $3\sigma$ by 5 eV, and from $1\pi$ by 13 eV. This set correlates mainly with the five metal $4d$ orbitals. This suggests the existence of different classes of configurations (see Table I), separated energetically and related to the different clusters in the following way:

(1) The first class of configurations (A to C) results from the occupation of the $\{1\delta, 2\pi, 4\sigma\}$ orbitals with a single electron. The three doublet states $X\,^2\Delta$, $A\,^2\Pi$, and $B\,^2\Sigma^+$ arise from cluster (I).
(2) The second class of configurations (D to F) corresponds to a single electron promotion $3\sigma \rightarrow \{1\delta, 2\pi, 4\sigma\}$, giving rise to 9 doublet and 4 quartet states. As observed in HfCl,[10] the electrostatic interaction strongly stabilizes (by about 8000 cm$^{-1}$) the quartet states with respect to the doublets. The two resulting clusters (II and III) regroup the quartets and doublets, respectively. Calculations have been carried out for all these states except the $3\,^2\Delta$ state arising from (F). The position of the $2\,^2\Sigma^+$ state, drawn with a dotted line in Fig. 3, is estimated using the vertical CMRCI energy (12 600 cm$^{-1}$) calculated at $R = 2.35$ Å.
(3) The third class of configurations (G to I) involves double excitations $3\sigma 1\delta \rightarrow \{2\pi, 4\sigma\}$ and leads to 2 quartets and 6 doublets. The doublet spin system (cluster V) is again significantly higher than the quartet (cluster IV), and has not been considered in our calculations.
(4) The next class of configurations, coming from $3\sigma^2 \rightarrow \{1\delta, 2\pi, 4\sigma\}$ excitations, also leads to two clusters (VI and VII) of 5 quartets and 18 doublets, respectively. The doublet cluster is again outside of the range of our calculations, while the 3 low-lying quartets ($^4\Delta$, $^4\Pi$, and $^4\Phi$) have been calculated.

TABLE I. Spectroscopic properties of the low-lying electronic states of ZrCl, from CMRCI calculations (see Figs. 1–3). Experimental values from previous work (Refs. 2, 11) or this work are given in parentheses.

| State | | | | | |
|---|---|---|---|---|---|
| (Old labels) | (New labels) | Cluster[a] | $T_0$ (cm$^{-1}$) | $R_e$ (Å) | $\omega_e$ (cm$^{-1}$) |
| $a\,^2\Phi$ | $X\,^2\Delta$ | I | 0 | 2.367 | 366 |
| | | | | (2.284) | (413.5) |
| | $A\,^2\Pi$ | I | 1504 | 2.408 | 360 |
| | $B\,^2\Sigma^+$ | I | 4708 | 2.439 | 338 |
| | $C\,^2\Sigma^-$ | III | 7597 | 2.463 | 354 |
| $[7.3]^2\Delta$ | $D\,^2\Phi$ | III | 7737 | 2.472 | 331 |
| | | | (7300) | (2.375) | (362.6)[b] |
| | $E\,^2\Pi$ | III | 8292 | 2.465 | 328 |
| $[9.4]^2\Phi$ | $F\,^2\Delta$ | III | 9429 | 2.476 | 336 |
| | | | (9370) | (2.370) | (355.4) |
| | $1\,^2\Gamma$ | III | 9767 | 2.416 | 351 |
| | $3\,^2\Pi$ | III | 11108 | 2.455 | 334 |
| | $2\,^2\Phi$ | III | 12315 | 2.442 | 341 |
| $X\,^4\Phi$ | $a\,^4\Phi$ | II | 616 | 2.458 | 334 |
| | | | (1200)[c] | (2.366) | (382)[d] |
| | $b\,^4\Sigma^-$ | II | 963 | 2.438 | 336 |
| | $c\,^4\Pi$ | II | 2188 | 2.466 | 328 |
| $C\,^4\Delta$ | $d\,^4\Delta$ | II | 4050 | 2.489 | 310 |
| | | | (5320) | (2.385) | ⋯ |
| | $2\,^4\Sigma^-$ | IV | 7082 | 2.476 | 335 |
| | $2\,^4\Pi$ | IV | 10740 | 2.527 | 300 |
| | $2\,^4\Delta$ | VI | 11338 | 2.545 | 298 |
| | $3\,^4\Pi$ | VI | 12774 | 2.518 | 303 |
| | $2\,^4\Phi$ | VI | 13279 | 2.561 | 286 |

[a]See Table III and Fig 3.
[b]The $\Delta G(1/2)$ value.
[c]From deperturbation calculation, see text for details.
[d]Estimated value of the $X\,^2\Delta_{3/2} - a\,^4\Phi_{3/2}$ energy difference, see text and Fig. 7.

The configuration mixing appearing in the CMRCI wave functions (see Table III) can also be interpreted in terms of the clustering. One observes that the secondary configurations having the larger weights are generally those arising from neighboring clusters within the same spin system. One sees for instance that wave functions belonging to cluster (III) are mixed with those of cluster (V), with significant weights (between 10% and 30%) for the corresponding configurations. The negligible mixing between clusters (III) and

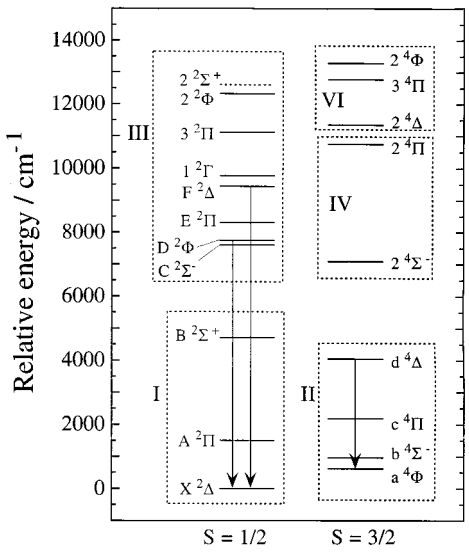


FIG. 3. Relative energies within the doublet and quartet spin systems of ZrCl from CMRCI calculations. See text and Table III for a definition of the clusters of levels, labeled I, II, III, IV, and VI. The arrows indicate previously measured infrared electronic transitions (Refs. 2, 11, 12).

(VII) is an indication of the larger energy separation between these two clusters, mainly due to the large $3\sigma$–$1\delta$ energy gap.

One can predict, by extrapolating the above analysis, that the next configuration class should arise from the single excitation $1\pi \rightarrow \{1\delta, 2\pi, 4\sigma\}$, with a new pair of clusters (VIII and IX), made of 8 quartets and 18 doublets, respectively. The magnitude of the $3\sigma$–$1\pi$ separation (8 eV) suggests these clusters to be significantly higher than the lower ones. Cluster VIII is of particular interest for the present study because it is from configuration $1\sigma^2 2\sigma^2 1\pi^3 3\sigma^2 1\delta^1 2\pi^1$ that the $^4\Gamma$ state seen in our laser excitation spectrum arises.

One sees in Fig. 3 that the electrostatic repulsion between the doublet (III) and quartet (II) states pushes down the latter cluster to energies close to those of cluster I. The $^4\Phi$ and $^2\Delta$ states are thus very close together, but our calculations predict the $^2\Delta$ state to be more stable by 616 cm$^{-1}$ ($T_0$ value, see Table I) than the $^4\Phi$ state. This confirms the *ab initio* results of Sakai *et al.*,[1] who calculated this energy difference to be of 710 cm$^{-1}$ at a similar level of theory. These authors also calculated the second excited state ($a\,^4\Sigma^-$) at 839 cm$^{-1}$, also in agreement with our value of 963 cm$^{-1}$. Sakai *et al.* did not calculate the location of any other excited states. Our work is thus the first *ab initio* investigation of the electronic states of ZrCl up to 14 000 cm$^{-1}$, and we refer to Table I for the calculated spectroscopic properties of the 19 low-lying electronic states.

## V. ELECTRONIC STRUCTURE OF THE ISOVALENT TiCl, ZrCl, AND HfCl MOLECULES

It seems now well established on experimental and theoretical grounds[1,7,8,9,10] that the transition metal chlorides TiCl, ZrCl, and HfCl have different ground electronic states. This suggests that in spite of their isovalent nature, they may have quite different electronic structures. This motivated us to make a comparative *ab initio* investigation of the valence electronic structure along the series TiCl→ZrCl→HfCl.

Our previous CMRCI results[10] provide most of the information for HfCl needed to achieve this goal, in particular the energy ordering within clusters I, II, and III. Additional vertical term energy calculations were performed at $R = 2.4$ Å, close to the equilibrium geometry of most valence states of HfCl, on the $2\,^4\Pi$ and $2\,^4\Sigma^-$ states belonging to cluster IV, and on the low-lying state of cluster VI ($3\,^4\Pi$). The CMRCI relative energies are 10 830, 13 700, and 25 400 cm$^{-1}$, for the $2\,^4\Pi$, $2\,^4\Sigma^-$, and $3\,^4\Pi$ states, respectively. One obtains in this way the following energy ordering for the low-lying states of HfCl:

$$^2\Delta < ^2\Pi < ^2\Sigma^+ < ^4\Phi < ^4\Delta < ^4\Sigma^- < ^4\Pi < ^4\Pi < ^4\Sigma^- < ^2\Sigma^- < ^2\Phi < ^2\Gamma < ^2\Pi < ^2\Delta < ^2\Sigma^+ < ^2\Pi < ^2\Phi < ^4\Pi. \quad (1)$$

In the case of TiCl, for which no *ab initio* information was available for all the states of clusters I, II, III, and IV, we

TABLE II. Electronic configurations describing the low-lying electronic states of ZrCl (see Table III).

| Label | Configuration[a] | Electron promotion[b] | Arising states |
|---|---|---|---|
| (A) | $1\sigma^2 2\sigma^2 1\pi^4 3\sigma^2 1\delta^1$ | | $^2\Delta$ |
| (B) | $1\sigma^2 2\sigma^2 1\pi^4 3\sigma^2 2\pi^1$ | $1\delta \rightarrow 2\pi$ | $^2\Pi$ |
| (C) | $1\sigma^2 2\sigma^2 1\pi^4 3\sigma^2 4\sigma^1$ | $1\delta \rightarrow 4\sigma$ | $^2\Sigma^+$ |
| (D) | $1\sigma^2 2\sigma^2 1\pi^4 3\sigma^1 1\delta^1 2\pi^1$ | $3\sigma \rightarrow 2\pi$ | $^2\Pi(2)$, $^2\Phi(2)$, $^4\Pi$, $^4\Phi$ |
| (E) | $1\sigma^2 2\sigma^2 1\pi^4 3\sigma^1 1\delta^2$ | $3\sigma \rightarrow 1\delta$ | $^2\Gamma$, $^2\Sigma^+$, $^2\Sigma^-$, $^4\Sigma^-$ |
| (F) | $1\sigma^2 2\sigma^2 1\pi^4 3\sigma^1 1\delta^1 4\sigma^1$ | $3\sigma \rightarrow 4\sigma$ | $^2\Delta(2)$, $^4\Delta$ |
| (G) | $1\sigma^2 2\sigma^2 1\pi^4 3\sigma^1 2\pi^2$ | $3\sigma\,1\delta \rightarrow 2\pi^2$ | $^2\Delta$, $^2\Sigma^+$, $^2\Sigma^-$, $^4\Sigma^-$ |
| (H) | $1\sigma^2 2\sigma^2 1\pi^4 3\sigma^1 4\sigma^2$ | $3\sigma\,1\delta \rightarrow 4\sigma^2$ | $^2\Sigma^+$ |
| (I) | $1\sigma^2 2\sigma^2 1\pi^4 3\sigma^1 2\pi^1 4\sigma^1$ | $3\sigma\,1\delta \rightarrow 2\pi\,4\sigma$ | $^2\Pi(2)$, $^4\Pi$ |
| (J) | $1\sigma^2 2\sigma^2 1\pi^4 1\delta^2 2\pi^1$ | $3\sigma^2 \rightarrow 1\delta\,2\pi$ | $^2H$, $^2\Phi$, $^2\Pi(2)$, $^4\Pi$ |
| (K) | $1\sigma^2 2\sigma^2 1\pi^4 1\delta^2 4\sigma^1$ | $3\sigma^2 \rightarrow 1\delta\,4\sigma$ | $^2\Gamma$, $^2\Sigma^+$, $^2\Sigma^-$, $^4\Sigma^-$ |
| (L) | $1\sigma^2 2\sigma^2 1\pi^4 1\delta^3$ | $3\sigma^2 \rightarrow 1\delta^2$ | $^2\Delta$ |
| (M) | $1\sigma^2 2\sigma^2 1\pi^4 1\delta^1 2\pi^2$ | $3\sigma^2 \rightarrow 2\pi^2$ | $^2\Gamma$, $^2\Delta(2)$, $^2\Sigma^+$, $^2\Sigma^-$, $^4\Delta$ |
| (N) | $1\sigma^2 2\sigma^2 1\pi^4 1\delta^1 4\sigma^2$ | $3\sigma^2 \rightarrow 4\sigma^2$ | $^2\Delta$ |
| (O) | $1\sigma^2 2\sigma^2 1\pi^4 1\delta^1 2\pi^1 4\sigma^1$ | $3\sigma^2 \rightarrow 2\pi\,4\sigma$ | $^2\Pi(2)$, $^2\Phi(2)$, $^4\Pi$, $^4\Phi$ |

[a]Configurations are classified by types of electron excitations.
[b]Electron promotions are defined with respect to the ground electronic configuration (A).

TABLE III. Analysis of the CMRCI wave function of ZrCl in terms of electronic configurations.[a,b]

| Cluster | Electronic state | Weight |
|---|---|---|
| I | $X\ ^2\Delta$ | 74% (A)+11% (F)+2% (G)+2% (N) |
| | $A\ ^2\Pi$ | 60% (B)+20% (D)+5% (I)+4% (J) |
| | $B\ ^2\Sigma^+$ | 41% (E)+30% (C)+7% (H)+6% (G)+3% (K) |
| II | $a\ ^4\Phi$ | 94% (D) |
| | $b\ ^4\Sigma^-$ | 68% (E)+26% (G) |
| | $c\ ^4\Pi$ | 83% (D)+10% (I) |
| | $d\ ^4\Delta$ | 95% (F) |
| III | $C\ ^2\Sigma^-$ | 65% (E)+12% (G)+14% (K) |
| | $D\ ^2\Phi$ | 89% (D)+3% (O)+2% (J) |
| | $E\ ^2\Pi$ | 80% (D)+5% (J)+4% (I)+2% (B) |
| | $F\ ^2\Delta$ | 64% (F)+18% (G)+4% (A)+2% (L) |
| | $1\ ^2\Gamma$ | 88% (E)+3% (K) |
| | $3\ ^2\Pi$ | 63% (D)+14% (B)+6% (O)+4% (I)+4% (J) |
| | $2\ ^2\Phi$ | 84% (D)+6% (O) |
| | $2\ ^2\Sigma^+$ | 34% (C)+28% (E)+17% (G)+7% (H)+3% (K) |
| IV | $2\ ^4\Sigma^-$ | 68% (G)+25% (E) |
| | $2\ ^4\Pi$ | 61% (I)+18% (J)+10% (D)+4% (O) |
| VI | $2\ ^4\Delta$ | 93% (M) |
| | $3\ ^4\Pi$ | 46% (J)+22% (I)+24% (O) |
| | $2\ ^4\Phi$ | 92% (O) |

[a]Weights (in percent) are obtained from the square of the corresponding configuration interaction coefficients; weights lower than 2% are not reported.
[b]See Table II for the definition of the configuration labels.

have performed CMRCI calculations at a single geometry of 2.3 Å, also close to the equilibrium geometries in this system. The lowest state of cluster VI($2\ ^4\Delta$) has also been calculated. The resulting energy ordering for TiCl is

$$^4\Phi<^4\Sigma^-<^4\Pi<^4\Delta<^2\Delta<^2\Phi<^2\Pi<^2\Sigma^-<^2\Sigma^+<^4\Sigma^- <^2\Pi<^4\Delta<^2\Delta<^2\Gamma<^2\Sigma^-<^2\Pi<^4\Pi<^2\Phi \quad (2)$$

with the corresponding relative vertical energies of 0, 880, 1532, 2593, 3517, 4479, 5035, 5363, 7200, 7987, 8277, 9146, 10076, 11574, 11804, 12046, 12478, and 13991 $cm^{-1}$.

The corresponding energy sequence (see Table I) for ZrCl is

$$^2\Delta<^4\Phi<^4\Sigma^-<^2\Pi<^4\Pi<^4\Delta<^2\Sigma^+<^4\Sigma^-<^2\Sigma^-<^2\Phi <^2\Pi<^2\Delta<^2\Gamma<^4\Pi<^2\Pi<^4\Delta<^2\Phi<^4\Pi<^4\Phi. \quad (3)$$

The comparison between sequences (1)–(3) can be visualized in Fig. 4, where the relative energy scales for the 3 molecules are shown. The origin of each individual scale has been fixed to the lower $^2\Delta$ state, in order to better discuss the energy shifts along the series. The electronic levels are regrouped in clusters I–VI, as defined in the previous section and in Ref. 10. No state labels are indicated on this figure in order to make it clearer, this information being explicitly given in sequences (1)–(3). The evolution along the series indicates that

(i) Except for slight internal energy changes, cluster I is almost identical in all systems;
(ii) Clusters II and III move to higher energies when going from TiCl to HfCl. These shifts can be quantified by the following changes in the average clusters energies from TiCl to HfCl,
Cluster (II): $-3560\rightarrow570\rightarrow5450\ cm^{-1}$,
Cluster (III): $5120\rightarrow8290\rightarrow15760\ cm^{-1}$,
these energies being relative to the corresponding average energies in cluster (I) and calculated taking the space and spin degeneracies into account. One sees that clusters II and III, arising from the same class of configurations, undergo significant shifts of similar size which means that the doublet-quartet splitting is of the same order of magnitude (8680, 7720, and 10300 $cm^{-1}$);
(iii) Cluster IV is also moving up, but to a lesser extent, the average energies with respect to cluster I being $6120\rightarrow8000\rightarrow9470\ cm^{-1}$.

The above findings give a simple interpretation of the differences observed between the electronic spectra of the three chlorides, in terms of the energy shift of clusters II–III with respect to cluster I. This explains why the ground state changes along the TiCl, ZrCl, HfCl series from $X\ ^4\Phi$ to $X\ ^2\Delta$, with ZrCl having nearly isoenergetic $X\ ^2\Delta$ and $a\ ^4\Phi$ states.

A deeper understanding of these changes needs a comparative investigation of the wave functions, as summarized in Table IV. This table reports the results of a Mulliken

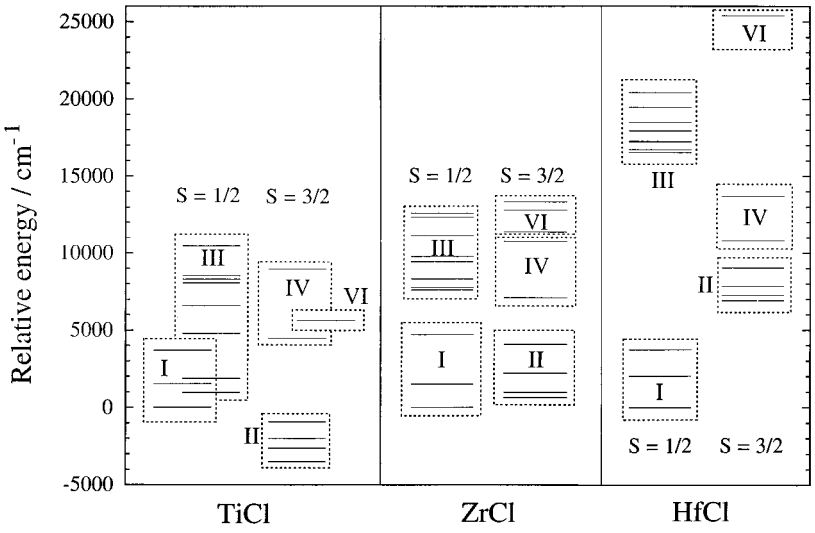


FIG. 4. Comparison of the low-lying electronic structure of the isovalent TiCl, ZrCl, and HfCl molecules from CMRCI calculations. The electronic states are regrouped into clusters, as detailed in the text (see also Fig. 3 and Table III for ZrCl and Ref. 10 for HfCl). Only the lowest state of cluster VI has been calculated for TiCl and HfCl, while the 3 low-lying states are shown for ZrCl. The origin of the energy scale within each system is defined with respect to the lowest $^2\Delta$ state.

TABLE IV. Comparative analysis of the lowest energy $^2\Delta$ and $^4\Phi$ wave functions of MCl molecules (M=Ti, Zr, and Hf).

| | | $^2\Delta$ | | | $^4\Phi$ | | |
|---|---|---|---|---|---|---|---|
| | | Ti | Zr | Hf | Ti | Zr | Hf |
| Populations[a] | $s_M$ | 1.07 | 1.59 | 1.62 | 0.87 | 0.46 | 0.93 |
| (in electrons) | $p_M$ | 0.20 | 0.09 | 0.31 | 0.27 | 0.17 | 0.25 |
| | $d_M$ | 2.09 | 1.72 | 1.52 | 2.18 | 2.65 | 2.2 |
| | $s_{Cl}$ | 2.00 | 2.02 | 2.01 | 1.99 | 2.01 | 2 |
| | $p_{Cl}$ | 5.63 | 5.56 | 5.54 | 5.67 | 5.69 | 5.61 |
| Ionicity[b] | $\delta$[b,c] | 0.64 | 0.60 | 0.55 | 0.68 | 0.72 | 0.62 |
| Dipole moment (in D)[c] | $\mu$ | 4.04 | 3.25 | 3.40 | 4.80 | 4.92 | 4.34 |
| Configuration mixing[d] | $a^2$ | 98 | 55 | 45 | 86 | 44 | 89 |
| | $b^2$ | 2 | 45 | 55 | 14 | 56 | 11 |

[a]Gross Mulliken atomic populations on *s*-, *p*-, and *d*-type atomic orbitals, calculated from full-valence CASSCF calculations.
[b]Ionic charge on atoms $M^{+\delta}Cl^{-\delta}$.
[c]Calculated from CMRCI calculations.
[d]Square of atomic configuration mixing coefficients [see Eqs. (4) and (5)], calculated from CASSCF atomic populations (in %, see text).

atomic population analysis performed on full-valence CASSCF wave functions describing the two lowest energy $^2\Delta$ and $^4\Phi$ states.

An important factor is the degree of ionicity of the different chlorides, which can be described[1,10] as $M^{+\delta}Cl^{-\delta}$ (with M=Ti, Zr or Hf). The atomic fractional charge $\delta$ is calculated as the difference between the total gross populations on the atoms of a given chloride and the actual charges of the corresponding isolated atoms. The $\delta$ values vary from 0.55 to 0.72 electron charges, with the following trends: (i) the ionicity is larger in the $^4\Phi$ state than in the $^2\Delta$ state, as already pointed out by Sakai *et al.*;[1] (ii) the ionicity decreases slightly from TiCl to HfCl. These trends are confirmed by the values of the expectation values of the dipole moment operator, also reported in Table IV. The dipole moments (in debye) have been calculated from the CMRCI wave functions at internuclear distances close to the equilibrium positions in the different states. Notice the high values of the dipole moment at equilibrium for these ionic molecules.

Another interesting property is the relative *s*-, *p*-, and *d*-type populations on both atoms, which changes significantly for the different chlorides and also from one electronic state to another. The populations on *f*-type orbitals of *X* and on *d*-type orbitals of chlorine are negligible (lower than 0.004 and 0.03 electron charges, respectively) and are not reported. One sees that the populations on chlorine are almost constant, but that the major changes are in the *s* and *d* populations on the M atom. The sum of the *s*- and *d*-type populations is, however, close to 3 suggesting the distribution of 3 electrons in the valence *s* and *d* orbitals of an $M^+$ cation. The correlation of the low-lying electronic states of MCl with those of $M^+$ thus seems reasonable, as already discussed previously for similar systems.[6,10,23,24] In this simple model of ionic bonding, an $M^+$ cation is subjected to the electric field of a $Cl^-$ ligand. Referring to atomic data tables,[25] $Ti^+$, $Zr^+$, and $Hf^+$ actually have three mixed low-lying electronic configurations resulting from the occupation of the close-lying $(n+1)s$ and $nd$ orbitals (with $n=3$, 4, and 5 for $Ti^+$, $Zr^+$, and $Hf^+$, respectively) by 3 electrons, i.e., the $(n+1)s\ nd^2$, $(n+1)s^2\ nd$, and $nd^3$ configurations. The lowest $^4\Phi$ state necessarily correlates with a $^4$F atomic state which can arise only from $(n+1)s\ nd^2$ or $nd^3$, while the lowest $^2\Delta$ state could correlate with different states arising from the three different atomic configurations. Explicit correlations demonstrate that only the $(n+1)s\ nd^2$, and $(n+1)s^2\ nd$ atomic configurations are candidates for forming the $^2\Delta$ states. It follows that the MCl electronic wave functions can be approximated by the following two-configuration mixed wave functions.

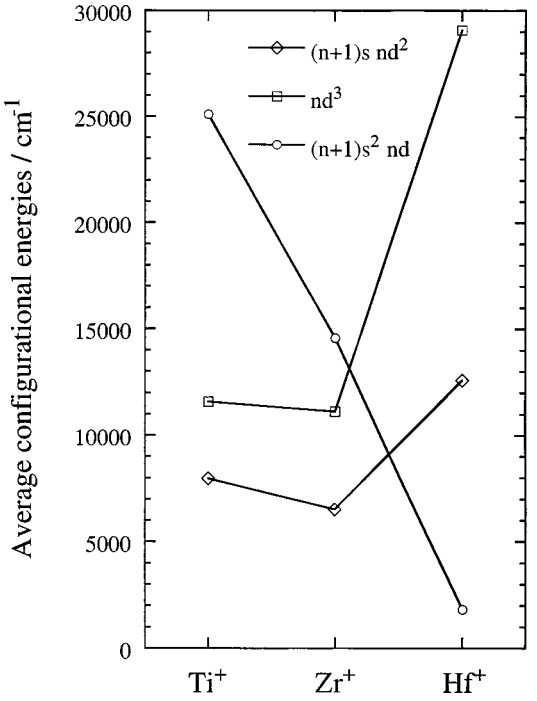


FIG. 5. Evolution of the average energies (Ref. 25) of configurations $(n+1)s\ nd^2$, $(n+1)s^2nd$, and $nd^3$ along the sequence $Ti^+ \rightarrow Zr^+ \rightarrow Hf^+$ (with $n=3$, 4, and 5, respectively), to be correlated to TiCl, ZrCl, and HfCl (see text).

$$|s^n d^m(^4\Phi)\rangle = a|s\ d^2\rangle + b|d^3\rangle, \tag{4}$$

$$|s^n d^m(^2\Delta)\rangle = a|s\ d^2\rangle + b|s^2\ d\rangle, \tag{5}$$

where *n* and *m* refer to the $s_M$ and $d_M$ populations, respectively (see Table IV) and *a* and *b* are normalized mixing coefficients. The squares of coefficients *a* and *b*, giving the weights of $M^+$ configurations in an MCl compound, are reported in Table IV. They show that the $^2\Delta$ state of TiCl has a pure $Ti^+(sd^2)$ character, while the $^2\Delta$ of $Zr^+$ and $Hf^+$ have nearly equal $(sd^2)$ and $(s^2d)$ mixing. As for the $^4\Phi$ state, $Ti^+$ and $Hf^+$ have a major $(sd^2)$ character, while $Zr^+$ exhibits a nearly equal mixture of $(sd^2)$ and $(d^3)$. This interpretation is consistent with the changes in the electronic structure of the singly charged ions, along the series $Ti^+ - Zr^+ - Hf^+$, as illustrated in Fig. 5. This figure shows the change of the average configuration energies along the series, calculated from experimental atomic data.[25] One sees that $(sd^2)$ and $(d^3)$ are crossed by $(s^2d)$ in the vicinity of $Zr^+$, and that $(d^3)$ is strongly destabilized in $Hf^+$. This atomic data explains why

TABLE V. Comparative analysis of the low-lying doublet CMRCI wave functions (cluster I) of TiCl, ZrCl, and HfCl in terms of electronic configurations.[a,b]

| Molecule | Electronic state | Weight |
|---|---|---|
| TiCl | $a\,^2\Delta$ | 35% (A)+54% (F)+3% (N) |
| | $b\,^2\Pi$ | 91% (D) |
| | $c\,^2\Sigma^+$ | 63% (E)+14% (G)+10% (H)+5% (C) |
| ZrCl | $X\,^2\Delta$ | 74% (A)+11% (F)+2% (G)+2% (N) |
| | $A\,^2\Pi$ | 60% (B)+20% (D)+5% (I)+4% (J) |
| | $B\,^2\Sigma^+$ | 41% (E)+30% (C)+7% (H)+6% (G)+3% (K) |
| HfCl[c] | $X\,^2\Delta$ | 84% (A)+2% (G)+4% (F) |
| | $A\,^2\Pi$ | 78% (B)+9% (D) |
| | $B\,^2\Sigma^+$ | 78% (C)+8% (H)+7% (E) |

[a]Weights (in percent) are obtained from the square of the corresponding configuration interaction coefficients; weights lower than 2% are not reported.
[b]See Table II for the definition of the configuration labeling.
[c]See Ref. 10.

(i) For $Ti^+$ in TiCl the $^2\Delta$ state is dominated by the $(sd^2)$ configuration and the $^4\Phi$ state arises from $(sd^2)$ with a slight mixing with $(d^3)$;
(ii) For $Zr^+$ in ZrCl both states exhibit mixed configurations;
(iii) For $Hf^+$ in HfCl the $^2\Delta$ state presents a similar $(sd^2)-(s^2d)$ mixing as in $Zr^+$, while the $^4\Phi$ state has a dominant $(s^2d)$ character.

The above analysis is qualitative, but it helps explain the differences in the lowest $^2\Delta$ and $^4\Phi$ states in TiCl, ZrCl, and HfCl. The other excited states considered in this work have similar changes that can be correlated to the cluster shifts illustrated in Fig. 4.

An analysis of the CASSCF molecular orbitals of the three chlorides indeed demonstrates that the $(n+1)s$ and $nd$ orbitals of M correlate to $3\sigma$ and $\{1\delta, 2\pi, 4\sigma\}$ orbitals, respectively, in MCl. This means roughly (see Table II) that configurations A–C (cluster I of ZrCl) should correspond to $M^+(s^2d)$, configurations D–I (clusters II–V) to $M^+(sd^2)$ and configurations J–O (clusters VI and VII) to $M^+(d^3)$. This approximately matches the evolution observed in Fig. 4. Clusters II–IV are at similar energies in $Ti^+$ and $Zr^+$, but are pushed to higher energies in $Hf^+$, following the $(sd^2)$ change in Fig. 5. The first state of cluster VI also follows the $(d^3)$ variation: it is close to cluster IV in $Ti^+$ and $Zr^+$ and is pushed to higher energy in $Hf^+$. The situation is more intricate for cluster I, which undergoes internal changes that can be related to the $(sd^2)-(s^2d)$ crossing. One thus progressively changes the dominant contributions from $(sd^2)$ to $(s^2d)$ when going from TiCl to HfCl, with the intermediate mixed case for ZrCl. This is confirmed by the comparative analysis of the CMRCI wave functions presented in Table V. Notice also in Fig. 4 that, because of the strong mixing, clusters I–III and IV–VI of TiCl are interpenetrated.

Given the qualitative agreement of the above $MCl \rightarrow M^+$ correlation, it is tempting to go a step further. One can expect in TiCl that the ground state cluster II ($^4\Phi, ^4\Sigma^-, ^4\Pi, ^4\Delta$) correlates to the ground $^4F(sd^2)$ state of $Ti^+$, and that the lower states of clusters I ($^2\Delta$ and $^2\Pi$) and III ($^2\Phi$ and $^2\Sigma^-$) correlate to the $a\,^2F(sd^2)$ state of $Ti^+$. This correlation is not too bad, if one compares the $^4F-^2F$ average term energy separation in $Ti^+$ (4500 $cm^{-1}$) to the difference of average clusters energies in TiCl (3200 $cm^{-1}$). In the same way, in HfCl, the ground cluster I ($^2\Delta, ^2\Pi, ^2\Sigma^+$) is to be correlated to the $a\,^2D(s^2d)$ state of $Hf^+$, and cluster II ($^4\Phi, ^4\Delta, ^4\Sigma^-, ^4\Pi$) to the $a\,^4F(sd^2)$ state of $Hf^+$. The difference of the average clusters energies in HfCl (6200 $cm^{-1}$) is again close to the average term energy separation in $Hf^+$ (4500 $cm^{-1}$). Similar correlations are less clear in the case of ZrCl, due to the strong atomic configuration mixings already pointed out.

## VI. EXPERIMENTAL OBSERVATION AND ANALYSIS

After scanning the region of 425 nm to 398 nm, it was readily apparent that the signal from the *C* band system of ZrCl was not strong. Numerous trials with different gas mixtures and ablation laser energies were attempted to increase the signal with only a minor gain in the signal-to-noise ratio. The final optimum conditions are given in Sec. II above. It should be noted, however, that the ablation energy used is a factor of 2 and the reactant gas percentage is a factor of 4 greater than what we have normally used to create other metal chloride species such as TiCl, HfCl, CoCl, and YbCl. For this reason, the rotational temperature of the molecules in the molecular beam and perhaps the population of the vibrational levels are likely abnormal.

Four groups of bands, with heads corresponding to some of those seen by Carroll and Daly,[3] were seen. The wave numbers of the band heads agree fairly well with Ref. 3 (see Table VI) although Zr atomic lines did make measurements impossible in some instances. In terms of relative intensities, the bands near 24 105 $cm^{-1}$ and 24 155 $cm^{-1}$ were the strongest, the broad feature centered near 24 345 $cm^{-1}$ was weaker and the features near 24 517 $cm^{-1}$ were very weak. For the other transition metal chloride molecules created with this ablation source, and also some other diatomic molecules containing zirconium, i.e., ZrO and ZrN, strong signals have resulted in all cases for absorptions from the ground state. Therefore, because the observed ZrCl intensities were so weak, it is believed that the observed band systems do not involve the ground electronic state.

Unfortunately the bands were not rotationally resolved at our pulsed laser resolution. Due to the weak nature of the signals and the fact that the band positions lie outside the operating range of our Coherent ''Autoscan'' ring dye laser system, we were unable to get high resolution data for these bands. Rotationally-resolved spectra and the first lines of the bands would have made the characterization of the electronic states much easier. However, we have been able to use the prior TiCl, ZrCl, and HfCl, spectra and calculations, and the present *ab initio* calculations as a guide.

The ground state of TiCl is now known to be a $X\,^4\Phi$ state while that of HfCl has recently been determined to be a $X\,^2\Delta$ state. For ZrCl, there is some question as to whether the ground state is $^4\Phi$ or $^2\Delta$ since these states are nearly isoenergetic.[1] The weak spectra obtained here are clearly telling us that the lower state of the *C* band system is not the ground state. What is also clear is that there are 3 or more subbands involved. In this respect, our spectra support the

earlier work of Carroll and Daly.[3] We only see one of the systems reported by Jordan *et al.*,[5] a band which also is reported in Ref. 3. Clearly the number of subbands rules out $^2\Delta$ as the lower state. We therefore surmise that the lower state involved is the $^4\Phi$ state. One therefore expects four subbands in the electronic transition. This certainly coincides with the interpretations of both Carroll and Daly[3] and Jordan *et al.*[5] although the respective authors suggested a different lower state. Imajo and co-workers[4] have seen these four subbands at high resolution and suggest a $^4\Gamma-^4\Phi$ assignment.

Carroll and Daly[3] observed that the bands all belong to the 0–0 sequence and that there were certain regularities in the spectra: 9 $cm^{-1}$ and 14 $cm^{-1}$ spacings between two types of heads. We also see these approximate spacings in our head positions. We also do not see the presence of any $Zr^{37}Cl$ bands which supports their $\Delta v=0$ assignments. Our data combined with the 0–0 bands assigned by Carroll and Daly[3] allows us to find a spacing of $\sim$182 $cm^{-1}$ between four subbands. Therefore we can interpret the bands at 24 144, 24 328, 24 517, and 24 690 $cm^{-1}$ (Ref. 3) as four subbands arising from the $^4\Phi$ state. From the analysis of Carroll and Daly,[3] it is apparent that the 9 $cm^{-1}$ spacing is the spacing between the 0–0, 1–1, 2–2, etc. bands. This leaves the 14 $cm^{-1}$ interval to explain. One can envisage three types of electronic transitions from a $^4\Phi$ state: $^4\Gamma-^4\Phi$, $^4\Phi-^4\Phi$, and $^4\Delta-^4\Phi$. For these one expects *R*, *Q*, and *P* branches but of differing intensity. For the $^4\Gamma-^4\Phi$ transition, the *R*-branch will be stronger than the *P*-branch, the $^4\Phi-^4\Phi$ transition will have an *R*-branch approximately the same intensity as the *P*-branch, while the $^4\Delta-^4\Phi$ transition will have the *R*-branch weaker than the *P*-branch. Our spectra show a head 14 $cm^{-1}$ to the high wave number side and red-degraded in the same sense as the first head in the subband. This is consistent with an *R*-head to higher frequency of a *Q*-head. The heads would be violet-degraded if it were a *P*- and *Q*-head situation. There is no sign of a third branch which leads us to a prediction of a $^4\Gamma-^4\Phi$ transition with the *P*-branch being weak and therefore buried in the noise in our spectra. A representative spectrum is given in Fig. 6 where the 0–0 and 1–1 *Q*- and *R*-heads of the $^4\Gamma_{5/2}-a\,^4\Phi_{3/2}$ transition are indicated. The intensities of the heads are irregular but there are some reasonable explanations for this. The first is that the conditions used to create the ZrCl molecules are out of the ordinary. A higher ablation energy and a richer reactant gas mixture results in a ''hotter'' beam. This means that more lines will appear in the *R*-branches giving stronger *R*-heads. In addition, the 1–1 *Q*-head is lying on top of a portion of the 0–0 *R*-branch so the intensity of this *Q*-head is a combination of the two bands. The 0–0, 1–1, 2–2, etc. band systems lie quite close together, some 9 or so $cm^{-1}$ apart, so the position of the 2–2 *Q*-head will be underneath the 1–1 *R*-branch. This gives the 1–1 *R*-branch more intensity than expected. The weak feature to high frequency of the 1–1 *R*-head is most likely the 2–2 *R*-head which supports this explanation. It is also possible that the positions of the 0–0 and 1–1 bands might be switched, however, we see no evidence to support this. The final identification of the bands will have to wait for a complete rotational analysis.[4] A summary of our assignments of the various spectral features is given in Table VI. Comparisons with the previous assignments by Carroll and Daly[3] and Jordan *et al.*[5] are also given.

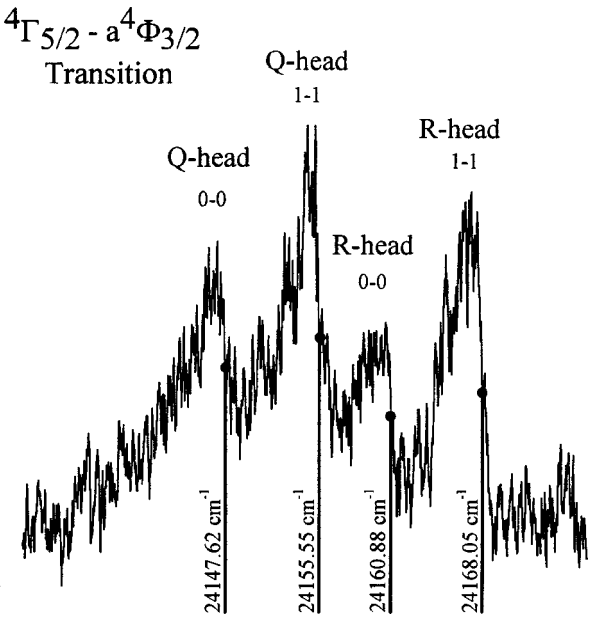


FIG. 6. The 0–0 and 1–1 *Q*- and *R*-heads for the $^4\Gamma_{5/2}-a\,^4\Phi_{3/2}$ electronic transition are shown.

Recently some FT spectra of ZrCl have been taken by Imajo and co-workers.[4] They have also observed the bands recorded by us and report that their analysis supports the assignment of a $^4\Gamma-^4\Phi$ transition. They also see the band which we have designated as $?-a\,^4\Phi_{3/2}$. We have given this band this designation because its intensity is almost identical to that of the $^4\Gamma_{5/2}-a\,^4\Phi_{3/2}$ subband. However, it does not fit with the $\Delta\Sigma=0$ subband assignments given here. It also does not fit with the idea of a $\Delta\Sigma\neq0$ spin–orbit component as the spin–orbit interval for the $^4\Phi$ state is $\sim$345 $cm^{-1}$ (see Discussion). The exact nature of this particular transition remains to be determined and, for example, a $^4\Sigma^-$ lower state can not be ruled out yet.

## VII. DISCUSSION

The ordering of the low-lying states can be estimated from the perturbations. Unfortunately the $X\,^2\Delta$ state does not display any sharp local perturbations, only global shifts in vibrational energy levels and rotational constants. Guided by *ab initio* calculations, these global interactions serve to locate the $a\,^4\Phi$ state relative to the $X\,^2\Delta$ state.

The $X\,^2\Delta$ state can interact directly with the $a\,^4\Phi$ state through the microscopic form of the spin–orbit operator,[26]

$$\hat{H}_{so}=\sum_i a_i\mathbf{l}_i\cdot\mathbf{s}_i=\sum_i a_i(\hat{l}_z\hat{s}_z+\tfrac{1}{2}(\hat{l}_+\hat{s}_-+\hat{l}_-\hat{s}_+))_i. \quad (6)$$

The $X\,^2\Delta$ state has $1\sigma^2 2\sigma^2 1\pi^4 3\sigma^2 1\delta^1$ as a dominant configuration (Table III) and $a\,^4\Phi$ is well represented as $1\sigma^2 2\sigma^2 1\pi^4 3\sigma^1 1\delta^1 2\pi^1$. The spin–orbit operator has a nonzero matrix element between $^4\Phi_{3/2}$ and $^2\Delta_{3/2}$,

TABLE VI. Measured band head positions in $cm^{-1}$.

| This work | Designation[a] | Ref. 3 | Designation | Ref. 5 | Designation |
|---|---|---|---|---|---|
| 24 104.6 | $?-a\ ^4\Phi_{3/2}$ | 24 104.9 | | | |
| 24 147.6 | $^4\Gamma_{5/2}-a\ ^4\Phi_{3/2}$, 0–0, *Q*-head | 24 144.5 | | | |
| 24 155.6 | $^4\Gamma_{5/2}-a\ ^4\Phi_{3/2}$, 1–1, *Q*-head | 24 155.3 | | | |
| 24 160.9 | $^4\Gamma_{5/2}-a\ ^4\Phi_{3/2}$, 0–0, *R*-head | 24 156.8 | | | |
| 24 168.1 | $^4\Gamma_{5/2}-a\ ^4\Phi_{3/2}$, 1–1, *R*-head | 24 168.1 | | | |
| b | $^4\Gamma_{7/2}-a\ ^4\Phi_{5/2}$, 0–0, *Q*-head | 24 328.6 | 0–0, $\beta$ | | |
| b | $^4\Gamma_{7/2}-a\ ^4\Phi_{5/2}$, 0–0, *R*-head | 24 343.8 | 0–0, $\alpha$ | | |
| 24 517.9 | $^4\Gamma_{9/2}-a\ ^4\Phi_{7/2}$, 0–0, *Q*-head | 24 517.3 | 0–0, $\beta$ | 24 517.5 | $^4\Pi_{3/2}-^4\Sigma$, 0–0, *Q*-head |
| c | $^4\Gamma_{9/2}-a\ ^4\Phi_{7/2}$, 1–1, *Q*-head | 24 525.5 | 1–1, $\beta$ | 24 525.6 | $^4\Pi_{3/2}-^4\Sigma$, 0–0, *R*-head |
| c | $^4\Gamma_{9/2}-a\ ^4\Phi_{7/2}$, 0–0, *R*-head | 24 530.4 | 0–0, $\alpha$ | | |
| 24 538.6 | $^4\Gamma_{9/2}-a\ ^4\Phi_{7/2}$, 1–1, *R*-head | 24 538.7 | 1–1, $\alpha$ | | |
| 24 542.5 | $^4\Gamma_{9/2}-a\ ^4\Phi_{7/2}$, 3–3, *Q*-head | 24 541.6 | 3–3, $\beta$ | 24 541.9 | $^4\Pi_{3/2}-^4\Sigma$, 1–1, *R*-head |
| | $^4\Gamma_{11/2}-a\ ^4\Phi_{9/2}$, 0–0, *Q*-head | 24 690.6 | 0–0, $\beta$ | 24 690.8 | $^4\Pi_{5/2}-^4\Sigma$, 0–0, *Q*-head |

[a]Designations are given according to interpretations of this work and those in Refs. 3 and 5.
[b]This band was broad, showed no distinct heads and was obscured by a Zr atomic line rendering its measurement difficult.
[c]Zr atomic line obscured these features.

$$H_{v*v}(3/2)=\langle v^*;{}^4\Phi_{3/2}|\hat{H}_{so}|X\,{}^2\Delta_{3/2};v\rangle$$
$$=\langle 1\bar{\delta}^1 3\bar{\delta}^1 2\bar{\pi}^1|\tfrac{1}{2}a\hat{l}_+\hat{s}_-|1\bar{\delta}^1 3\bar{\sigma}^1 3\sigma^1\rangle\langle v^*|v\rangle$$
$$=\sqrt{\frac{3}{2}}a\langle v^*|v\rangle \qquad (7)$$

assuming (see below, however) that the $3\sigma$ and $2\pi$ orbitals can be represented as $4d\sigma$ and $4d\pi$ orbitals, respectively. The bar over a spin–orbital indicates a $\beta(m_s=-1/2)$ spin function while the absence of a bar denotes an $\alpha(m_s=+1/2)$ spin function. The $\langle v^*|v\rangle$ integral is a vibrational overlap and $\langle v^*|v\rangle^2$ is a Franck–Condon factor. A similar equation holds for $\Omega=5/2$,

$$H_{v*v}(5/2)=\langle v^*;{}^4\Phi_{5/2}|\hat{H}_{so}|X\,{}^2\Delta_{5/2};v\rangle$$
$$=\langle 1\delta^1 3\bar{\sigma}^1 2\bar{\pi}^1|\tfrac{1}{2}a\hat{l}_+\hat{s}_-|1\delta^1 3\bar{\sigma}^1 3\sigma^1\rangle\langle v^*|v\rangle$$
$$=\sqrt{\frac{3}{2}}a\langle v^*|v\rangle. \qquad (8)$$

These $^4\Phi_{3/2}\sim{}^2\Phi_{3/2}$ and $^4\Phi_{5/2}\sim{}^2\Phi_{5/2}$ interactions are homogeneous (i.e., not *J* dependent) and strong because the spin–orbit constant, *a*, has a value of several hundred $cm^{-1}$ [$a=\zeta(4d)=363\,cm^{-1}$ for $Zr^+$].[26] The other spin components ($^4\Phi_{7/2}$, $^4\Phi_{9/2}$) of the $^4\Phi$ state cannot interact with the $^2\Delta$ state in this manner. As expected, the $^4\Phi_{7/2}$ and $^4\Phi_{9/2}$ spin-components do not display strong global perturbations, although the $^4\Phi_{9/2}$ spin-component does suffer from some unidentified, mainly local perturbations. The low-lying $b\ ^4\Sigma^-$ state does not have a first order interaction with either the $X\ ^2\Delta$ state or the $^4\Phi$ state, although higher order, weaker interactions are possible.

The energy level diagram deduced from our observations is given as Fig. 7. The $X\ ^2\Delta_{3/2}$ and $X\ ^2\Delta_{5/2}$ vibrational intervals were known from our previous high resolution work but only a low resolution vibrational interval $\sim$380 $cm^{-1}$ is available for the $^4\Phi_{3/2}$ spin component. The vibrational constants for the $^4\Phi$ state were taken as $\omega_e=382\,cm^{-1}$ and $\omega_e x_e=1.1\,cm^{-1}$. The value for $\omega_e x_e$ is an estimate based on other ZrCl states. The $v=0$ and 1 levels of $X\ ^2\Delta_{3/2}$ and $X\ ^2\Delta_{5/2}$ spin-components are unperturbed and $v=2$ of $X\ ^2\Delta_{3/2}$ is only very slightly affected. The ''unperturbed'' vibrational constants for the $X\ ^2\Delta$ state are approximately $\omega_e=413.8$ and $\omega_e x_e=1.2\,cm^{-1}$. The unperturbed rotational constants are $B_e=0.128\,53$, $\alpha_e=0.000\,54$ for $X\ ^2\Delta_{3/2}$ and $B_e=0.128\,36\,cm^{-1}$, $\alpha_e=0.000\,54\,cm^{-1}$ for $X\ ^2\Delta_{5/2}$. The shifts from the expected vibrational levels and in the rotational constants are shown in Fig. 7. For the $^4\Phi_{3/2}$ and $^4\Phi_{5/2}$ no vibrational shifts could be deduced experimentally, although they are presumably equal and opposite to the corresponding $^2\Delta_{3/2}$ and $^2\Delta_{5/2}$ shifts, respectively. The shifts, however, in the rotational constants of the $^4\Phi_{3/2}$ and $^4\Phi_{5/2}$ spin components could be deduced from the relatively unperturbed $^4\Phi_{7/2}$ and $^4\Phi_{9/2}$ values.

The shifts in the *B* values are shown in $B_{obs}-B_{calc}$ and the shifts in energy levels are $G(v)_{obs}-G(v)_{calc}$. The shifts in energy levels places the $v=0$ $a\ ^4\Phi_{3/2}$ level just below the $v=3$ $X\ ^2\Delta_{3/2}$ level. Similarly $v=0$ and 1 of the $a\ ^4\Phi_{5/2}$ state lie between $v=2$ and 3 of the $X\ ^2\Delta_{5/2}$ state. The shifts in *B* values are equal and opposite in sign consistent with a simple mixing of the electronic wave functions. Application of second order perturbation theory puts $v=0$ $a\ ^4\Phi_{3/2}$ about 30 $cm^{-1}$ ($\pm10$ $cm^{-1}$) below $v=3$ $X\ ^2\Delta_{3/2}$. Similarly $v=0$ of $a\ ^4\Phi_{5/2}$ state lies about 20 $cm^{-1}$ ($\pm10$ $cm^{-1}$) above $v=2$ $X\ ^2\Delta_{5/2}$, as shown in Fig. 7.

The effective, unperturbed *B* values give an estimate of about 705 $cm^{-1}$ (Fig. 7) for the $^2\Delta_{5/2}$ to $^2\Delta_{3/2}$ spin–orbit intervals. The corresponding calculations[2] for the $^4\Phi_{5/2}$ to $^4\Phi_{3/2}$ interval gives a value of about $190\,cm^{-1}(3A)$. The energy difference implied by Fig. 7 for this same interval is 345 $cm^{-1}$. Not surprisingly the estimates for the spin–orbit intervals based on the effective *B* values are not very reliable.

The estimate for the spin–orbit constant *A* for the $X\ ^2\Delta$ state of ZrCl is, $A=a=\zeta(4d)=363\,cm^{-1}$. The spin–orbit interval, $\Delta E=E(^2\Delta_{5/2})-E(^2\Delta_{3/2})=2A=726\,cm^{-1}$ is de-

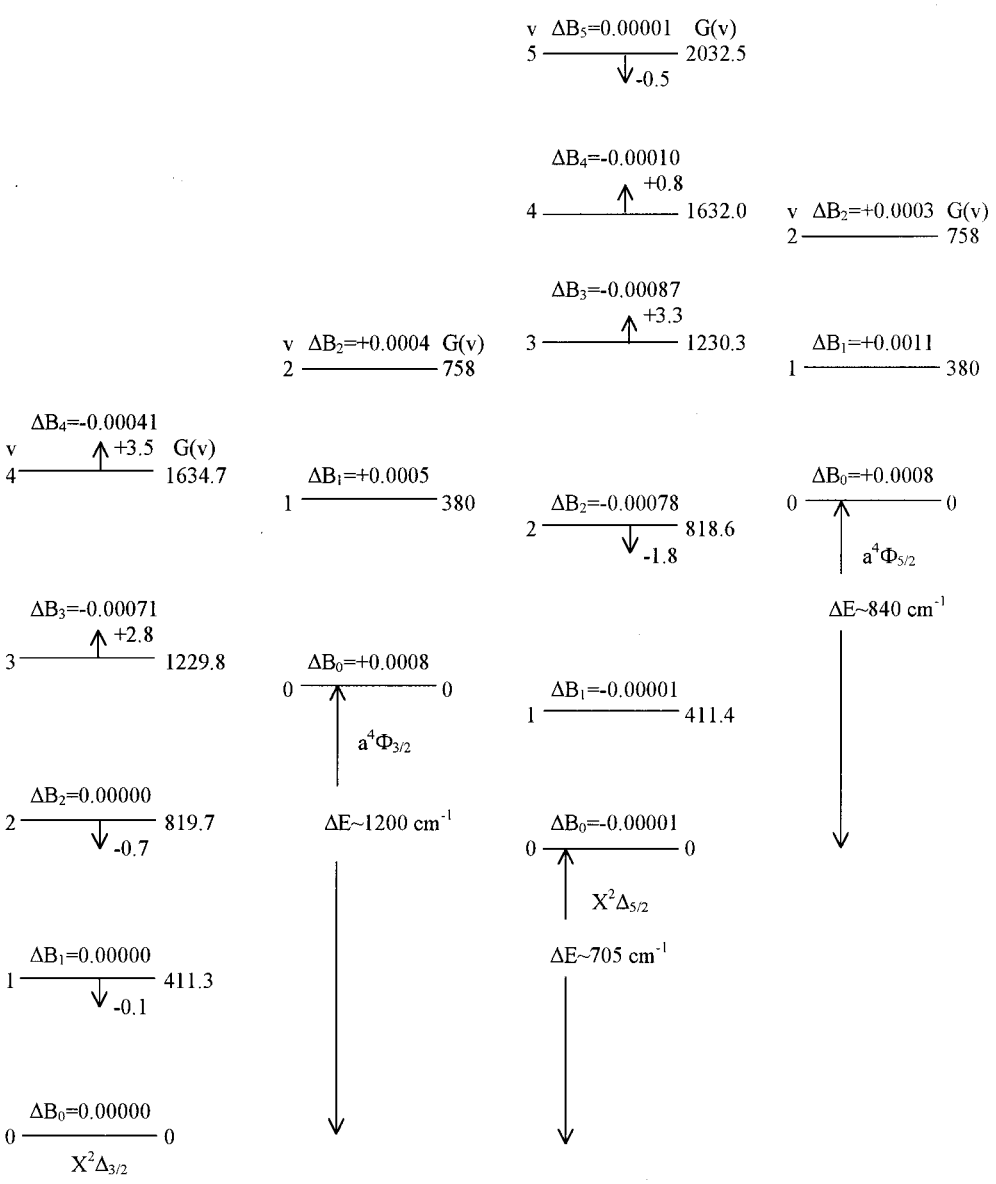


FIG. 7. A schematic diagram of the low-lying vibrational levels of ZrCl and their interactions.

rived using the atomic $\zeta(4d)$ tabulated by Lefebvre-Brion and Field[13] for $Zr^+$. This is comfortingly close to the value of 705 $cm^{-1}$ derived from the effective $B$ values. This also suggests that the spin–orbit interval $E(a\,^4\Phi_{5/2})-E(a\,^4\Phi_{3/2})=345\,cm^{-1}$ implied by Fig. 7 is relatively reliable ($\pm 30$ $cm^{-1}$).

The size of the perturbation matrix elements can also be estimated by calculating the unperturbed $\langle v=0;{}^4\Phi_{3/2}|{}^2\Delta_{3/2};v=3\rangle=0.16$ overlap integrals. Substituting in Eq. (7) leads to a value of 71 $cm^{-1}$ to compared with a value of about 8 $cm^{-1}$ estimated from second order perturbation theory. Similar calculations of $\langle v=0;{}^4\Phi_{5/2}|{}^2\Delta_{5/2};v=2\rangle=0.36$ lead to an estimated perturbation matrix element of 150 $cm^{-1}$ to be compared to an ''observed'' value of about 6 $cm^{-1}$. The agreement is not very good, presumably mainly because mixing of both orbitals and configurations. In particular, the assumption that the $3\sigma$ orbital is pure $4d\sigma$ is not very good because the correlation of $3\sigma$ to $5s$ and $4\sigma$ to $4d$ is more realistic. This mixing of orbitals and configurations, confirmed by our *ab initio* calculations, serves to decrease the value of the interaction matrix elements. Our simple calculations thus give the maximum possible value for the matrix elements rather than realistic estimates.

Our extensive *ab initio* data can now be used to propose a revision of the assignment of the previously reported near infrared transitions.[2,11] The old and new labels are given in the two first columns of Table I. The experimental values of spectroscopic constants are also given in parentheses. Most values come from previous work.[2,11] Notice that some $\omega_e$ values have been estimated (see above) or correspond to a $\Delta G_{1/2}$ value. Also notice that a value of 1200 $cm^{-1}$ for the $X\,^2\Delta_{3/2}-a\,^4\Phi_{3/2}$ energy separation has been estimated from a deperturbation calculation (see above), compared to the *ab initio* term value of 606 $cm^{-1}$ for the $a\,^4\Phi$ state. The general agreement between experiment and theory is good, with a similar accuracy as in our previous work on HfCl,[10] i.e., within 0.1 Å for the equilibrium distances, within 50

$cm^{-1}$ for the harmonic frequencies and within 1300 $cm^{-1}$ for the term values. As already pointed out in HfCl,[10] the calculated $R_e$ values are systematically overestimated. Notice, however, that the significant increase (about 0.1 Å) in the bond distance, when going from the ground to the excited states, is correctly reproduced by the *ab initio* calculation. This suggests a systematic shift that could be due to an overestimation of some repulsive effects by the electron core potential. Both experiment and theory thus now support the following assignment for the previously observed near infrared transitions: $C\,^2\Phi - X\,^2\Delta$, $E\,^2\Phi - X\,^2\Delta$, and $d\,^4\Delta - a\,^4\Phi$.

Our reassignments of ZrCl also have implications for TiCl. The transition of TiCl near 12 800 $cm^{-1}$ that we assigned as $[12.8]^2\Phi - a\,^2\Phi$ may well be the $g\,^2\Delta - a\,^2\Delta$ transition analogous to the ZrCl transition. This transition is calculated to be at 6559 $cm^{-1}$, but we can not rule out the $k^2\Phi - b^2\Phi$ assignment calculated to be at 10 474 $cm^{-1}$.

## ACKNOWLEDGMENTS

We thank M. Dulick and C. Plymate of the National Solar Observatory for assistance in obtaining the spectra. The National Solar Observatory is operated by the Association of Universities for Research in Astronomy, Inc., under contract with the National Science Foundation. The research described here was supported by funding from the NASA laboratory astrophysics program. Some support was also provided by the Natural Sciences and Engineering Research Council of Canada. J. L. thanks the Fonds National de la Recherche Scientifique de Belgique and A. T. the Fondation Van Buuren for financial support. We thank T. Imajo for discussions and for sharing his TiCl and ZrCl results with us prior to publication.

[1] Y. Sakai, K. Mogi, and E. Miyoshi, J. Chem. Phys. **111**, 3989 (1999).
[2] R. S. Ram and P. F. Bernath, J. Mol. Spectrosc. **186**, 335 (1997).
[3] P. K. Carroll and P. J. Daly, Proc. R. Ir. Acad. Sect. A, Math. Astron. Phys. Sci. **61A**, 17 (1961).
[4] T. Imajo (private communication); T. Imajo, D. Wang, K. Tanaka *et al.*, J. Mol. Spectrosc. **203**, 216 (2000).
[5] K. J. Jordan, R. H. Lipson, N. A. McDonald, and D. S. Young, Chem. Phys. Lett. **193**, 499 (1992).
[6] R. S. Ram and P. F. Bernath, J. Mol. Spectrosc. **186**, 113 (1997).
[7] A. Maeda, T. Hirao, P. F. Bernath, and T. Amano, Paper, 55th International Symposium on Molecular Spectroscopy, June 2000.
[8] A. I. Boldryrev and J. Simons, J. Mol. Spectrosc. **188**, 138 (1998).
[9] C. Focsa, M. Bencheikh, and L. G. M. Pettersson, J. Phys. B **31**, 2857 (1998).
[10] R. S. Ram, A. G. Adam, A. Tsouli *et al.*, J. Mol. Spectrosc. **202**, 116 (2000).
[11] R. S. Ram and P. F. Bernath, J. Mol. Spectrosc. **196**, 235 (1999).
[12] J. G. Phillips, S. P. Davis, and D. C. Galehouse, Astrophys. J., Suppl. **43**, 417 (1980).
[13] C. Focsa (private communication).
[14] R. S. Ram, J. D. Peers, Y. Teng *et al.*, J. Mol. Spectrosc. **184**, 186 (1997).
[15] F. M. Phelps, *MIT Wavelength Tables, Wavelengths by Element* (MIT Press, Cambridge, MA, 1982), Vol. 2.
[16] H.-J. Werner and P. J. Knowles, J. Chem. Phys. **89**, 5803 (1988); P. J. Knowles and H.-J. Werner, Chem. Phys. Lett. **145**, 514 (1988).
[17] H.-J. Werner and P. J. Knowles, J. Chem. Phys. **82**, 5053 (1985); P. J. Knowles and H.-J. Werner, Chem. Phys. Lett. **115**, 259 (1985).
[18] S. R. Langhoff and E. R. Davidson, Int. J. Quantum Chem. **8**, 62 (1974).
[19] D. Andrae, U. Häussermann, M. Dolg *et al.*, Theor. Chim. Acta **77**, 123 (1990).
[20] A. Bergner, M. Dolg, W. Kuechle *et al.*, Mol. Phys. **80**, 1431 (1993).
[21] M. Dolg, U. Wedig, H. Stoll, and H. Preuss, J. Chem. Phys. **86**, 866 (1987).
[22] MOLPRO is a package of *ab initio* programs written by H.-J. Werner and P. J. Knowles, with contributions from J. Almlöf, R. D. Amos, A. Berning *et al.*
[23] R. S. Ram and P. F. Bernath, J. Mol. Spectrosc. **195**, 299 (1999).
[24] J. Anglada, P. J. Bruna, and S. D. Peyerimhoff, Mol. Phys. **69**, 281 (1990).
[25] C. E. Moore, *Atomic Energy Levels* (National Bureau of Standards, Washington, D.C., 1949), Vol. I; *ibid.*, Vol. II; *ibid.*, Vol. III.
[26] Lefebvre-Brion and R. W. Field, *Perturbations in the Spectra of Diatomic Molecules* (Academic, Orlando, 1986).